Inorganic Chemistry

pubs.acs.org/IC

Article

Isocyanide Ligands Promote Ligand-to-Metal Charge Transfer Excited States in a Rhenium(II) Complex

Tayliz M. Rodriguez, Mawuli Deegbey, Chun-Hsing Chen, Elena Jakubikova,* and Jillian L. Dempsey*

Cite This: *Inorg. Chem.* 2023, 62, 6576−6585

Read Online

ACCESS | Metrics & More | Article Recommendations | Supporting Information

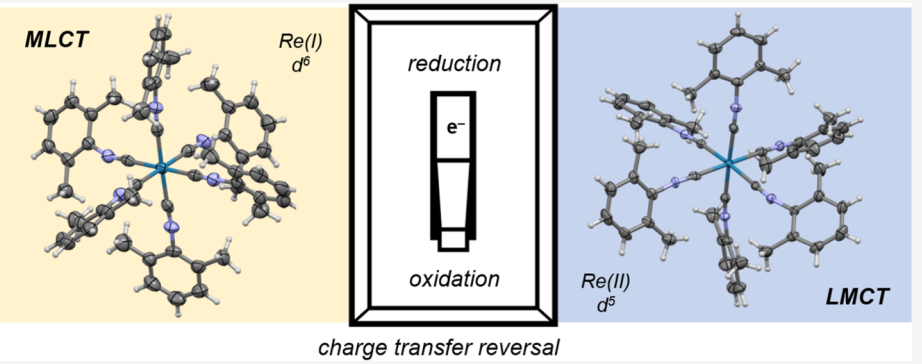

ABSTRACT: A metal-to-ligand charge transfer with mixed intraligand character is observed for the rhenium hexakisarylisocyanide complex $[Re(CNAr)_6]PF_6$ (CNAr = 2,6-dimethylphenylisocyanide, λ_{max} = 300 nm). Upon oxidation to $[Re(CNAr)_6](PF_6)_2$, the dominant low energy optical transition is a ligand-to-metal charge transfer (LMCT) mixed with intraligand transitions (λ_{max} = 650 nm). TD-DFT was used to identify the participating ligand-based orbitals in the LMCT transition, revealing that the majority of the donor orbital is based on the aryl ring (85%) as opposed to the CN bond (14%). For both $[Re(CNAr)_6]^+$ and $[Re(CNAr)_6]^{2+}$, structural characterization by X-ray diffraction reveals deviations from O_h geometry at the central Re ion, with larger reduction in symmetry observed for Re(II). For $[Re(CNAr)_6]^+$, these structural changes lead to a broadening of the strong ν(C≡N) stretch (2065 cm^{-1}), as the degeneracy of the T_{1u} IR-active mode is broken. Furthermore, a shoulder is observed for this ν(C≡N) stretch, resulting from deviation of the C−N−Ar bond from linearity. By contrast, $[Re(CNAr)_6]^{2+}$ has two weak bands in the ν(C≡N) region (2065 and 2121 cm^{-1}). DFT calculations indicate that reduction of symmetry at the central rhenium ion manifests in the decrease in intensity and the observed split of the ν(C≡N) band. Stability of both complexes are limited by light-induced decomposition where Re(I) dissociates a isocyanide ligand upon irradiation and Re(II) absorbance decays under ambient light. These data provide new insights to the electronic structure of $[Re(CNAr)_6]^{2+}$, enhancing our understanding of LMCT excited states and the versatility of isocyanide ligands.

INTRODUCTION

Isocyanide ligands serve as stronger σ-donors and weaker π-acceptors when compared to analogous CO.[1] The sterics and electronics of these ligands can be readily tuned through varying substituents, which is inaccessible to CO, and ultimately affects the degree of σ-donor and π-acceptor character.[2] This mixed behavior renders isocyanides far superior in stabilizing coordinately unsaturated complexes and unusual oxidation states.[3−7]

Isocyanide ligands engage in charge transfer behavior when coordinated to transition metals. For example, in a series of hexakisphenylisocyanide (CNPh) complexes $[M(CNPh)_6]^{n+}$ [where M = Cr(0), Mo(0), W(0) (n = 0), and Mn(I) (n = 1)], the dominant transitions are metal-to-ligand charge transfer (MLCT) excited states assigned as $d\pi(M) \rightarrow \pi^*(CNPh)$. Curiously, when $[Mn(CNPh)_6]^+$ is oxidized to $[Mn(CNPh)_6]^{2+}$, a low-energy ligand-to-metal charge transfer (LMCT) transition is observed and assigned as $\sigma(CNPh) \rightarrow d\pi(M)$.[8]

It has traditionally been understood that electron-rich molecules bearing π-acceptor ligands can access MLCT transitions, whereas electron-poor molecules with σ- and π-donor or other oxidizable ligands enable LMCT processes. Although there is a rich literature and countless examples of molecules with MLCT excited states,[9,10] coordination complexes with well-characterized LMCT excited states are

Received: September 8, 2022
Published: January 18, 2023

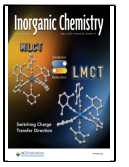

https://doi.org/10.1021/acs.inorgchem.2c03193
Inorg. Chem. 2023, 62, 6576−6585

Scheme 1. Synthesis of $[Re(CNAr)_6]PF_6$

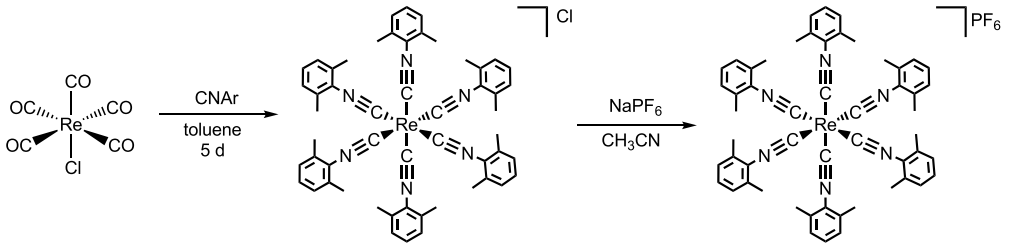

relatively rare.[11−17] Furthermore, there is a poor understanding of the orbital structure of ligands that can participate in LMCT transitions.[17,18] Thus, the switch between an MLCT excited state to an LMCT excited state upon oxidation of $[Mn(CNPh)_6]^+$ suggests rich orbital structures of isocyanide ligands.[8]

Hexacyano complexes $[M(CN)_6]^{(n+1)-}$ and their oxidized forms $[M(CN)_6]^{n-}$ [where M = Fe (n = 3) and Mn (n = 4)] exhibit charge transfer inversion from MLCT to LMCT upon oxidation, similar to the manganese hexakisphenylisocyanide complex introduced above.[19] The switch in charge transfer is rationalized by a half-filled t_{2g} orbital, promoting lower energy LMCT transitions when compared to the reduced complexes. Similarly, charge transfer inversion from MLCT to LMCT has also been observed upon oxidation of d^6 Fe(II) N-heterocyclic carbene (NHC) complexes to d^5 Fe(III) species.[14,20] Like isocyanides, the σ-donor and π-donor/acceptor properties of NHC ligands can facilitate charge transfer conversion based on the metal oxidation state, and as a result, stabilize high valent oxidation states.[21]

In order to enhance understanding of ligand orbital structure of isocyanides that enables LMCT transitions and provides enhanced characterization of LMCT excited states, we explored rhenium complexes with arylisocyanide ligands. The Re(I) complex $[Re(CNAr)_6]^+$ (CNAr = 2,6-dimethylphenylisocyanide) exhibits an emissive triplet MLCT excited state, with additional mixed character associated with intraligand (IL) charge transfer, at low temperatures.[22] In this work, we discover that like their manganese congeners, the rhenium hexakisarylisocyanide complexes exhibit a switch between MLCT and LMCT transitions when oxidized from Re(I) to Re(II). Investigations of the Re(II) hexakis(arylisocyanide) complex using a combination of spectroscopy and theory provide rich insights into the orbital structure of the isocyanide ligand that facilitates the LMCT transition.

EXPERIMENTAL SECTION

Computational Details. All optimized coordinates and computational methods are included in the Supporting Information.

General Considerations. All syntheses were performed under N_2 using standard Schlenk line techniques or in a N_2-filled glovebox unless otherwise stated. All solvents were dried and degassed with argon using a Pure Process Technology solvent system: dichloromethane (Sigma-Aldrich, anhydrous 99.8%), diethyl ether (Fisher Scientific, HPLC grade, 99%), and acetonitrile (VWR, ACS reagents). 1,2-Difluorobenzene (Oakwood Chemical, 99%) was dried over CaH_2 for 24 h, vacuum-transferred, and stored in the N_2-filled glovebox. $Re(CO)_5Cl$ (Sigma-Aldrich, 98%), 2,6-dimethylphenylisocyanide (CNAr; Sigma-Aldrich, 98%), and thianthrene (Th; Sigma-Aldrich, 97%) were used without further purification. Thianthrene radical cation, $[Th^{\bullet+}]PF_6$, was prepared following literature procedures, employing $NOPF_6$ instead of $NOBF_4$.[23]

^{1}H NMR were collected on a Bruker 400 MHz spectrometer at 295 K. UV/visible absorbance spectra were collected with an Agilent Cary 60 UV/vis spectrophotometer. High-resolution mass spectrometry was collected with a Thermo Scientific Q Exactive HF-X instrument.

Electrochemical Methods. Cyclic voltammograms were collected in a N_2-filled glovebox with a WaveDriver potentiostat (Pine Research). All voltammograms were recorded in a 0.25 M $[Bu_4N][PF_6]$ CH_3CN electrolyte solution using a three-electrode cell consisting of a 3 mm diameter glassy carbon working electrode, a glassy carbon counter electrode, and a Ag wire pseudo-reference electrode. All scans are referenced to the ferrocenium/ferrocene ($Fc^{+/0}$) couple.

FTIR Spectroscopy. Solid-state and solution infrared spectra were collected on a Thermo Scientific Nicolet iS5 FTIR equipped with a iD1 Transmission accessory for solution experiments using a liquid cell with CaF_2 windows.

Spectroelectrochemical Measurements. Infrared spectroelectrochemical experiments were performed with a gastight, optically transparent thin-layer solution IR cell fabricated by Prof. Hartl at the University of Reading, Reading, UK.[24] IR spectra were collected on a Thermo Scientific Nicolet iS5 FTIR equipped with an iD1 Transmission accessory. The cell contained a masked Au minigrid working electrode (32 wires/cm), a Pt gauze auxiliary electrode, and a Ag wire pseudo-reference electrode enclosed between CaF_2 windows. For all infrared spectroelectrochemical experiments, the solutions were prepared in a N_2-filled glovebox, and the sealed cell was brought outside the glovebox to collect data. To identify the appropriate potential window with the pseudo-reference electrode, a thin-layer cyclic voltammogram was recorded at 5 mV/s prior to the controlled potential electrolysis experiments. The subsequent controlled potential electrolysis experiment was performed with fresh analyte solution.

X-ray Crystallography. Single-crystal X-ray diffraction data was collected on a Bruker D8 VENTURE diffractometer at 150 K. Diffraction profiles were integrated using the SAINT (Bruker Analytical X-ray Systems, Madison, WI) software program. Absorption corrections were applied using SADABS.[25] The structures were solved using SHELXT[26] and refined (full-matrix least squares) using the Oxford University Crystals for Windows system.[27]

Synthesis of $[Re(CNAr)_6]Cl$. $[Re(CNAr)_6]Cl$ was prepared by modifying literature procedures.[22] Specifically, $Re(CO)_5Cl$ (0.513 g, 1.42 mmol), 2,6-dimethylphenylisocyanide (CNAr; 1.68 g, 12.8 mmol, 9 equiv), and 40 mL of toluene were added to a Schlenk flask. The colorless mixture was refluxed at 110 °C for 5 days under active N_2. After heating, the solution turned yellow and a pale yellow solid precipitated. The solid product was collected via filtration, dissolved in ethanol, and recrystallized via slow evaporation. Yield: 0.686 g, 64%. ATR-IR ν(CN) = 2066 cm^{-1}. ^{1}H NMR (400 MHz, $CDCl_3$): δ 7.17 (dd, H_{para}, 1H), 7.09 (d, H_{meta}, 1H), 2.42 (s, $-CH_3$, 6H) ESI-MS m/z = 973.396; calcd for $[Re(CNAr)_6]^+$ m/z = 973.4.

Synthesis of $[Re(CNAr)_6]PF_6$. The Cl^- counterion of $[Re(CNAr)_6]Cl$ was exchanged for PF_6^- via salt metathesis with $NaPF_6$. $[Re(CNAr)_6]Cl$ (0.192 g, 0.190 mmol) and $NaPF_6$ (0.033 g, 0.196 mmol) were dissolved in 10 mL of CH_3CN and stirred at room temperature for 2 h. After stirring, the solution was filtered and the filtrate was dried under vacuum to collect the product, $[Re(CNAr)_6]PF_6$. X-ray diffraction quality crystals were grown via vapor diffusion of Et_2O into a solution of $[Re(CNAr)_6]PF_6$ in 1,2-difluorobenzene at

https://doi.org/10.1021/acs.inorgchem.2c03193
Inorg. Chem. 2023, 62, 6576−6585

−35 °C. Yield: 0.198 g, 93%. FTIR (CH_3CN, CaF_2 windows, 25 °C) ν(CN) = 2065 cm^{-1}; ATR-IR ν(CN) = 2065 cm^{-1}. ^1H NMR (400 MHz, CD_2Cl_2): δ 7.18 (dd, H_{para}, 1H), 7.14 d (H_{meta}, 2H), 2.46 (s, $-CH_3$, 6H). ESI-MS m/z = 973.396; calcd for $[Re(CNAr)_6]^+$ m/z = 973.4; λ_{max} = 300 nm, $\varepsilon = 8.7 \times 10^4$ M^{-1} cm^{-1}.

Synthesis of $[Re(CNAr)_6](PF_6)_2$. $[Re(CNAr)_6]PF_6$ (0.132 g, 0.118 mmol) and $[Th^{\bullet+}]PF_6$ (0.042 g, 0.117 mmol) were dissolved in 6 mL of CH_3CN and stirred for 30 min. The pale yellow solution turns dark blue immediately upon addition of the oxidant. To isolate a solid product, the dark blue solution was dried under vacuum and washed with diethyl ether to remove the thianthrene byproduct. X-ray diffraction quality crystals were grown via vapor diffusion of Et_2O into a solution of $[Re(CNAr)_6](PF_6)_2$ in CH_2Cl_2 at −35 °C. Yield: 0.109 g, 74%. FTIR (CH_3CN, CaF_2 windows) ν(CN) = 2075 cm^{-1}. ESI-MS m/z = 486.696, calcd for $[Re(CNAr)_6]^{2+}$ m/z = 486.7.; λ_{max} = 650 nm, ε = 1286 M^{-1} cm^{-1}.

RESULTS AND DISCUSSION

$[Re(CNAr)_6]PF_6$ was synthesized through the reaction of $Re(CO)_5Cl$ with excess 2,6-dimethylphenylisocyanide (CNAr) in toluene, followed by salt metathesis with $NaPF_6$ in CH_3CN (Scheme 1). Previous reports for this complex used a multistep synthetic approach; first generating $Re(CNAr)_5Cl$ by refluxing $Re(CO)_5Cl$ with excess CNAr, then halide abstraction using AgOTf, and reacting 1 equiv of CNAr ligand and $[NH_4][PF_6]$ to form $[Re(CNAr)_6]PF_6$. Recently, a hexakisarylisocyanide Mn(I) complex, $[Mn(CNdippPh^{OMe2})_6]PF_6$ ($CNdippPh^{OMe2}$ = 4-(3,5-dimethoxyphenyl)-2,6-diisopropyl-phenylisocyanide), was synthesized through a similar approach—reacting phenylisocyanide with $Mn(CO)_5Br$ followed by salt metathesis in an aqueous hexafluorophosphate solution.[28] The ^1H NMR spectrum of $[Re(CNAr)_6]PF_6$ shows 6 equivalent isocyanide ligands—a single resonance (δ ppm 2.46) is observed for the methyl substituents on the aryl ring and a doublet and doublet-of-doublets are observed for the meta (H_{meta}, δ ppm 7.14) and para (H_{para}, δ ppm 7.18) protons of the ring. High-resolution mass spectrometry confirms the hexakis coordination by the isocyanide ligands [m/z = 973.396 (calcd m/z = 973.4 for $[Re(CNAr)_6]^+$); Figure S2].

X-ray diffraction quality crystals were grown via vapor diffusion of diethyl ether into a solution of the Re(I) complex in 1,2-difluorobenzene at −35 °C (Figure 1). Single-crystal X-ray diffraction data of the Re(I) homoleptic isocyanide complex features Re−C bond distances ranging from 2.026(7) to 2.052(7) Å. In comparison to $[Mn(CNdippPh^{OMe2})_6]PF_6$, the Re−C bond distances are slightly longer, consistent with a first row versus third row transition metal.[28] The C−Re−C bond angles ranging from 178.3(3) to 179.5(3)° and 88.5(2) to 91.5(3)° suggest that the complex has slightly distorted octahedral symmetry (see below). Similarly, this Mn(I) complex adopts a slightly distorted octahedral geometry.[28] Selected bond angles and distances are included in Table 1 (full crystallographic details are included in the Supporting Information). Though the hexakis Re(I) complex reported here has not been previously crystallized, the bond lengths of the equatorial CNAr ligands in $Re(CNAr)_5Cl$ are similar to those quantified for the hexakis complex. By contrast, $Re(CNAr)_5Cl$ adopts a slightly more distorted octahedral geometry than the hexakis species, with C−Re−C bond angles ranging from 173.7(2) to 176.1(2)°.

The solid-state FTIR spectra of $[Re(CNAr)_6]^+$ displays an intense isocyanide stretch ν(C≡N) at 2065 cm^{-1} (Figure 2), which correlates with the triply degenerate IR-active stretches (T_{1u} mode) for a complex of O_h symmetry. The IR stretch of

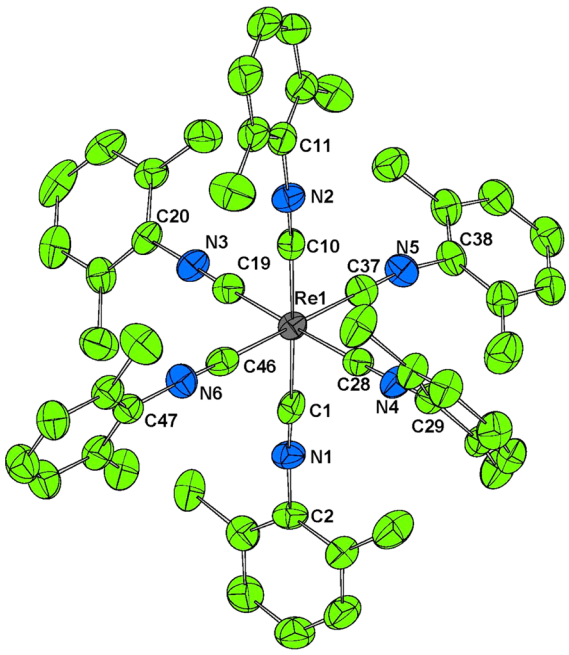

Figure 1. Ellipsoid plot at 50% probability for the molecular structure of $[Re(CNAr)_6]^+$. Solvent molecules, PF_6 counterion, and hydrogen atoms are omitted for clarity.

the free CNAr ligand is 2121 cm^{-1}, which upon coordination to Re shifts to lower frequency, indicating back-bonding from the metal (Figure S3). The Mn(I) complex $[Mn(CNdippPh^{OMe2})_6]PF_6$ exhibits a similar shift upon coordination from 2116 cm^{-1} for free ligand to 2070 cm^{-1}.[28] The manganese congener $[Mn(CNPh)_6]^+$ has a single isocyanide stretch at ν(C≡N) = 2080 cm^{-1}.[8] For further comparison, studies of $Re(CNR)_5Cl$ report a single IR-active isocyanide stretch at lower energy ν(C≡N) at 2044 cm^{-1}.[22] In addition to the strong stretch observed at 2065 cm^{-1} for $[Re(CNAr)_6]^+$, a weak lower energy shoulder is observed at 2004 cm^{-1}, which has been reported for several $[Mn(CNR)_6]^+$ complexes.[8,28,29] Deviation from linearity of the C−N−R bond that results from π-backing and changes in hybridization at the N atom lowers the symmetry, leading to this shoulder.[28,29] The C−N−Ar bond angles of $[Re(CNAr)_6]^+$ are not perfectly linear [163.9(6) to 172.8(7)°] and therefore correlate with this interpretation.

As noted above, a single IR-active C≡N band is predicted for an ideal octahedral complex, assigned to the triply degenerate T_{1u} mode. Experimentally a single band is observed for $[Re(CNAr)_6]^+$, but it is broad. $[Re(CNAr)_6]^+$ deviates from octahedral symmetry, as experimentally observed in the X-ray crystallography data. This results in splitting of the T_{1u} mode splitting into three non-degenerate C≡N stretching modes. Indeed, DFT vibrational analysis of $[Re(CNAr)_6]^+$ reveals three IR-active C≡N stretching modes at 2144, 2140, and 2134 cm^{-1} with absorptivity between 13343 and 13561 M^{-1} cm^{-1}, and three IR-inactive low intensity stretches at 2160, 2165, and 2261 cm^{-1}. The calculated IR-active ν(C≡N) stretch of the free ligand is 2190 cm^{-1}, which is of higher energy compared to the experimental stretching frequency [ν(C≡N) = 2121 cm^{-1}]. DFT is well known to systematically overestimate the IR frequencies, so the calculated frequencies are within the range of typical error for these types of calculations.[30] For the $[Re(CNAr)_6]^+$ complex, the three IR-

https://doi.org/10.1021/acs.inorgchem.2c03193
Inorg. Chem. 2023, 62, 6576−6585

Table 1. Select Bond Distances (Å) and Bond Angles of $[Re(CNAr)_6]^+$ and $[Re(CNAr)_6]^{2+}$

	bond length (Å)			<C−Re−C (deg)	
	$[Re(CNAr)_6]^+$	$[Re(CNAr)_6]^{2+}$		$[Re(CNAr)_6]^+$	$[Re(CNAr)_6]^{2+}$
Re1−C1	2.029(7)	2.048(9)	C1−Re1−C10	178.3(3)	177.3(3)
Re1−C10	2.042(7)	2.069(9)	C1−Re1−C19	90.4(3)	92.0(3)
Re1−C19	2.026(7)	2.068(8)	C10−Re1−C19	88.5(2)	86.2(3)
Re1−C28	2.031(7)	2.071(8)	C1−Re1−C28	90.2(2)	89.2(3)
Re1−C37	2.029(8)	2.059(9)	C10−Re1−C28	91.0(2)	92.4(3)
Re1−C46	2.052(7)	2.072(9)	C19−Re1−C28	178.7(3)	175.9(3)
N1−C1	1.168(8)	1.156(11)	C1−Re1−C37	91.5(3)	89.4(3)
N1−C2	1.400(8)	1.401(12)	C10−Re1−C37	89.7(2)	92.6(3)
N2−C10	1.168(8)	1.165(11)	C19−Re1−C37	89.3(3)	90.8(3)
N2−C11	1.395(8)	1.389(11)	C28−Re1−C37	89.6(3)	93.3(3)
N3−C19	1.172(8)	1.139(11)	C1−Re1−C46	88.3(2)	87.8(3)
N3−C20	1.406(8)	1.404(11)	C10−Re1−C46	90.5(2)	90.2(3)
N4−C28	1.169(8)	1.146(11)	C19−Re1−C46	88.3(2)	88.2(3)
N4−C29	1.394(8)	1.393(11)	C28−Re1−C46	90.8(2)	87.9(3)
N5−C37	1.169(8)	1.150(11)	C37−Re1−C46	179.5(3)	176.9(3)
N5−C38	1.405(8)	1.404(11)	C1−N1−C2	172.8(7)	168.6(9)
N6−C46	1.159(8)	1.145(11)	C10−N2−C11	172.7(7)	171.3(8)
N6−C47	1.393(8)	1.411(11)	C19−N3−C20	175.8(6)	174.9(9)
			C28−N4−C29	163.9(6)	167.3(8)
			C37−N5−C38	168.7(7)	176.0(9)
			C46−N6−C47	168.3(7)	172.4(9)

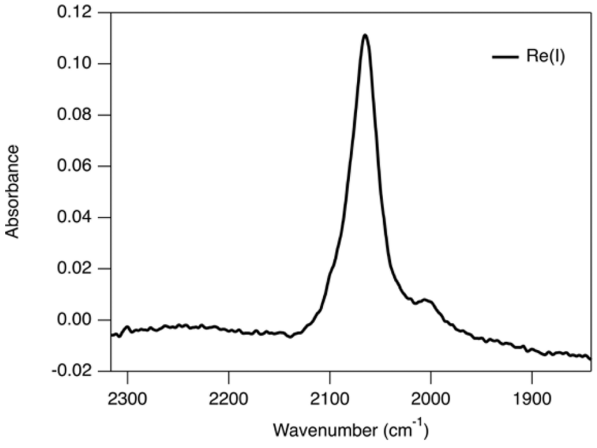

Figure 2. C≡N stretching region of the solid-state IR spectra of $[Re(CNAr)_6]PF_6$ [ν(C≡N) = 2065 cm^{-1}].

active −CN stretches are experimentally observed as a broad band in the simulated spectrum (Figures S19 and S20), which correlates with experimental observations (Figure 2). A broad C≡N stretch has also been reported for Mn(I) isocyanide complexes.[19,28,31] Similar to our findings here, this broadness has been ascribed to the deviations from octahedral geometry for hexakisisocyanide complexes and slight differences in metal−arylisocyanide bond lengths and angles, which result in breaking of degeneracy of the IR-active stretching modes to yield three energetically similar bands that are experimentally observed as a single broad peak.[28]

Solutions of $[Re(CNAr)_6]PF_6$ are pale yellow in color. The absorbance spectra of $[Re(CNAr)_6]PF_6$ is dominated by UV transitions (λ_{max} = 300 nm, $\varepsilon = 8.7 \times 10^4$ M^{-1} cm^{-1}),[22] which have been previously assigned as MLCT transitions that populate the ligand π^* orbitals mixed with IL charge transfer. Higher energy transitions have been assigned as ligand π to π^* transitions.[22] In this work, DFT was used to optimize the structures and TD-DFT was employed to assign the optical transitions of $[Re(CNAr)_6]^+$ (see computational details in the Supporting Information). The results show that the lowest energy transition at 352 nm (f = 0.0453) originates from a combination of two molecular orbitals of mixed character, HOMO − 2 (MO 215; 50% Re, 50% CNAr) and HOMO (MO 217; 47% Re, 53% CNAr), which both populate a ligand-based orbital LUMO (MO 218; 4% Re, 96% CNAr) (Figure 3). This transition corresponds to a mixture of IL and MLCT processes. The transition with the highest oscillator strength (f = 0.9299) at 312 nm also corresponds to a mixture of MLCT and IL (see Table S6 for the MO compositions). Similarly, the Mn(I) complex $[Mn(CNdippPh^{OMe2})_6]PF_6$ has two absorption bands in the UV region at 278 and 370 nm, which correspond to IL π to π^* CNR transitions and MLCT/IL, respectively.[31]

Thorough investigations of $[Mn(CNdippPh^{OMe2})_6]PF_6$ demonstrated that ligand photodissociation occurs when solutions of CH_3CN and CH_2Cl_2 were irradiated at 405 nm yielding complexes where one or two aryl isocyanides dissociated.[28] Similarly, $[Re(CNAr)_6]^+$ exhibits ligand photodissociation when irradiated with 365 nm light in CH_3CN. A decrease in absorbance of the UV features is observed, coupled to a red shift and growth of a new absorbance at 350 nm (Figure S6). Samples of irradiated $[Re(CNAr)_6]^+$ analyzed via HR-MS revealed the formation of a new species identified as $[Re(CNAr)_5(NCCH_3)]^+$ (m/z = 883.35; Figure S7) where one aryl isocyanide ligand has dissociated and acetonitrile has bound.

Cyclic voltammograms of $[Re(CNAr)_6]PF_6$ recorded in CH_3CN display a chemically and electrochemically reversible one-electron wave at 0.68 V versus $Fc^{+/0}$, assigned to the Re(II/I) couple across all scan rate studies (100−2000 mV/s) (Figure 4). A chemically irreversible oxidation is observed with $E_{p,a}$ = 1.5 V versus $Fc^{+/0}$, assigned to the Re(III/II) couple. The irreversibility of this feature at all scan rates studied (100−

https://doi.org/10.1021/acs.inorgchem.2c03193
Inorg. Chem. 2023, 62, 6576−6585

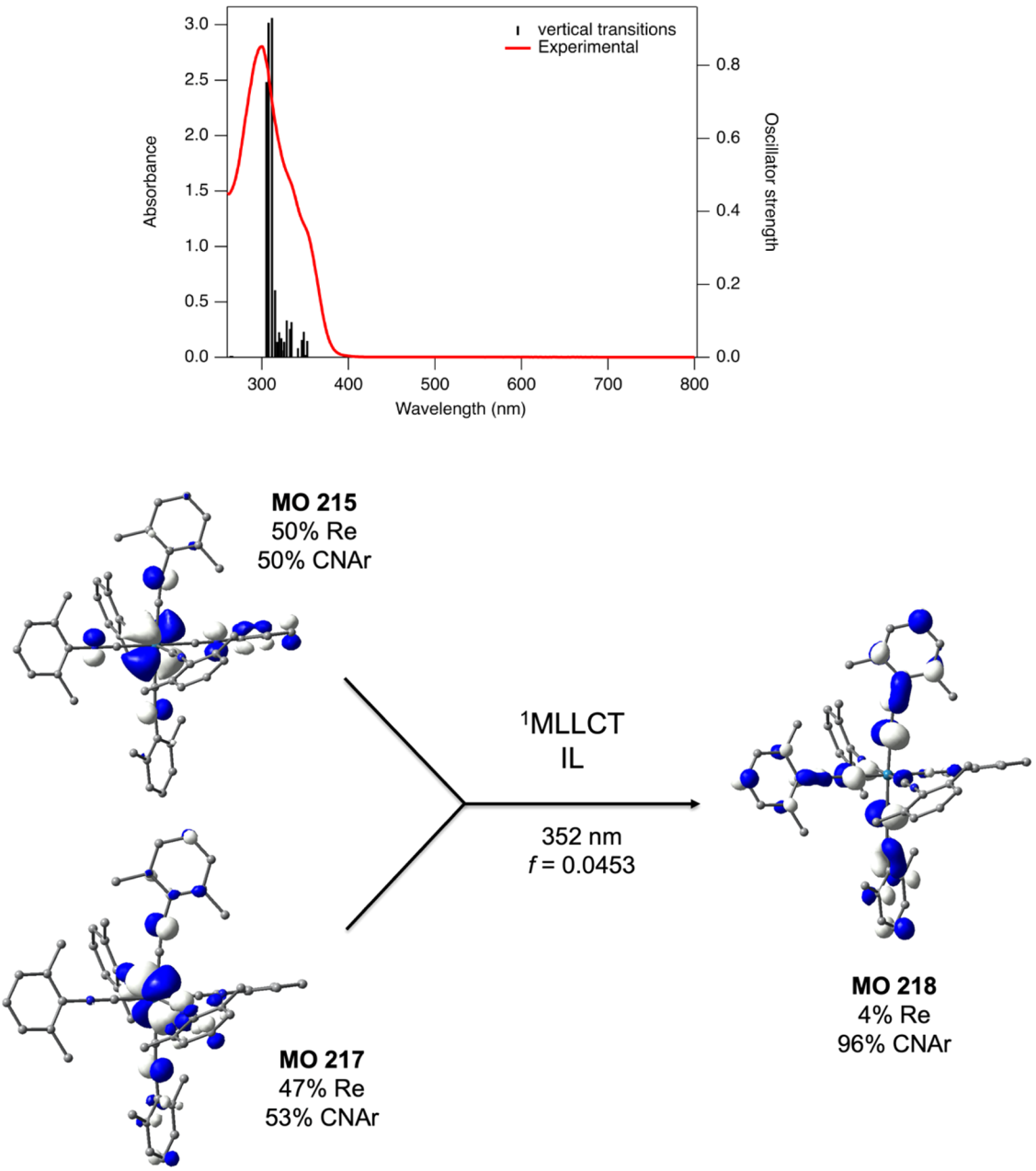

Figure 3. (Top) Experimental UV/vis spectrum of $[Re(CNAr)_6]PF_6$ in CH_3CN (red) and computed vertical transitions in CH_3CN using PCM solvation. (Bottom) The vertical lines represent the vertical transitions predicted via TD-DFT. The donor (MO 215 and 217) and acceptor (MO 218) orbitals participating in the dominant transition at 352 nm, which corresponds to a ^{1}MLCT/IL transition.

2000 mV/s) suggests that the 16-electron Re(III) species is unstable (Figure S5).

Based on the Re(II/I) reduction potential measured via cyclic voltammetry, the thianthrene radical cation ($[Th^{\bullet+}]$, $E_{1/2}$ = 0.86 V vs $Fc^{0/+}$ in CH_3CN) was selected for the chemical oxidation of Re(I) to Re(II).[32] $[Re(CNAr)_6]PF_6$ was reacted with $[Th^{\bullet+}]PF_6$ in CH_3CN to generate $[Re(CNAr)_6](PF_6)_2$ (Scheme 2). The thianthrene byproduct was removed with a diethyl ether wash.

Mass spectrometry confirms formation of the Re(II) product—half of the parent mass (m/z = 973.396) was observed as expected for a dicationic species (m/z = 486.696; Figure S4). Dark blue X-ray diffraction quality crystals were grown via vapor diffusion of diethyl ether into a solution of the Re(II) complex in CH_2Cl_2 at −35 °C. Structural characterization reveals subtle but important differences upon oxidation from Re(I) to Re(II) (Figure 5). Elongation is observed for the Re−C bond distances upon oxidation. $[Re(CNAr)_6]^{2+}$ features Re−C bond distances ranging from 2.048(9) to 2.072(9) Å. The C−N bond distances (C bound to Re) slightly decrease upon oxidation to Re(II) and the N−Ar bond distances remain relatively unchanged. Re−C bond elongation and C−N bond contraction in Re(II) are expected upon oxidation, as less π-back-bonding into the C≡N triple bond of the isocyanide ligands will occur in the higher oxidation state. Selected bond angles and distances are included in Table 1 (full crystallographic details in the Supporting Information).

Upon oxidation, the symmetry of the molecule around the Re center distorts further from octahedral. The C−Re−C core bond angles range from 175.9(3) to 177.3(3) and 86.2(3) to

https://doi.org/10.1021/acs.inorgchem.2c03193
Inorg. Chem. 2023, 62, 6576−6585

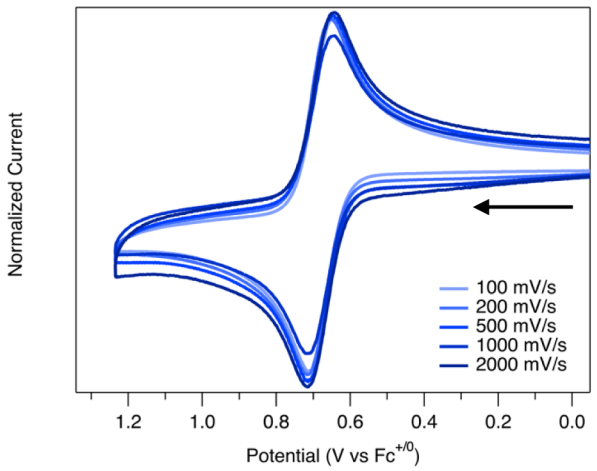

Figure 4. Cyclic voltammograms of 2.8 mM $[Re(CNAr)_6]PF_6$ in CH_3CN with 0.25 M $[Bu_4N][PF_6]$ as the supporting electrolyte under N_2. The current for each voltammogram is normalized by dividing the current by the square root of the scan rate ($i/v^{1/2}$). Arrow indicates direction scanned.

93.3(3)° in the Re(II) species. Another dramatic difference between the Re(I) and Re(II) structures is the C−N−Ar bond angles of the isocyanide ligands, which distort from angles ranging between 163.9(6) and 175.8(7)° in Re(I) to 167.3(8) to 176.0(9)° upon oxidation to Re(II) (Figure 6). The bond angles observed for C−N−Ar in the Re(II) complex are more linear in comparison to the Re(I) species, consistent with more back-bonding in the latter.

Oxidation of Re(I) to Re(II) results in a color change from pale yellow to dark blue. $[Re(CNAr)_6]^{2+}$ has a broad absorbance in the visible region with λ_{max} = 650 nm (ε = 1286 M^{-1} cm^{-1}; Figure 7). For comparison, $[Mn(CNPh)_6]^{2+}$ has been isolated as red crystals with λ_{max} = 490 nm at room temperature, and a second feature with λ_{max} = 548 nm observed at 77 K.[8] The stability of the Re(II) complex is limited by decomposition under ambient light and in solution, where the absorbance feature in the visible region is observed to decay over time (Figure S8).

DFT and TD-DFT were used to interrogate the electronic structure of the Re(II) complex. Geometry optimization of Re(II) was performed at the(U)B3LYP+D2/6-311G*, SDD level of theory and the Re−C and C−N bond lengths correlate with the experimental crystallographic data (see the Supporting Information). The calculated average Re−C and C−N bond distances show a slight deviation from experiment by 0.015 (0.01) and 0.001 (0.017) Å, respectively. TD-DFT at the same level of theory for the optimization was employed to simulate

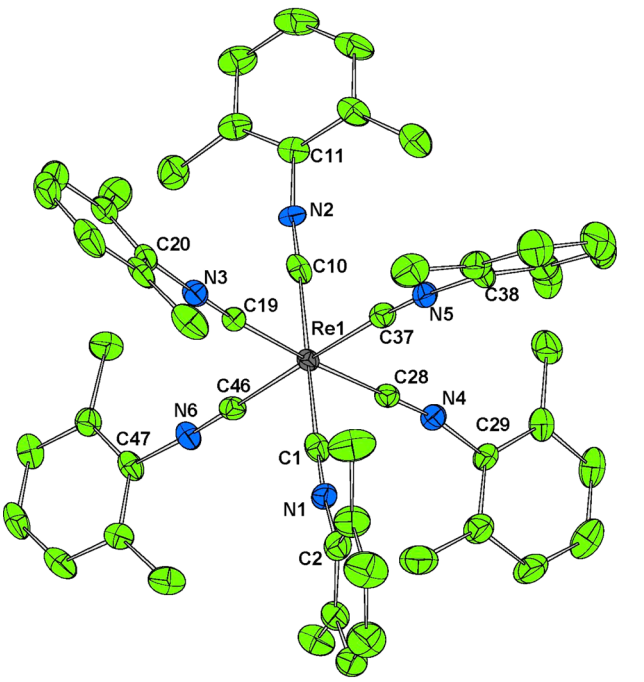

Figure 5. Ellipsoid plot at 50% probability for the molecular structure of $[Re(CNAr)_6]^{2+}$. Solvent molecules, PF_6 counterions, and hydrogen atoms are omitted for clarity.

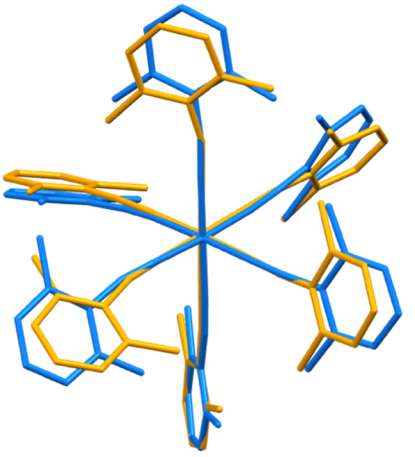

Figure 6. Overlay of Re(I) (orange) and Re(II) (blue) wireframe molecular crystal structures illustrating minimal distortions to core Re−C−N bonds. Distortions are observed in the aryl substituents of the arylisocyanide ligands (rmsd, 0.6254; max *D*, 1.6901 Å).

Scheme 2. Synthesis of $[Re(CNAr)_6](PF_6)_2$ Using the Thianthrene Radical Cation Oxidant

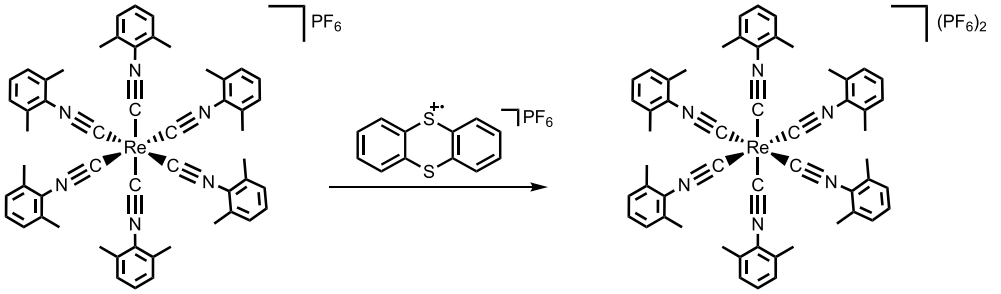

https://doi.org/10.1021/acs.inorgchem.2c03193
Inorg. Chem. 2023, 62, 6576−6585

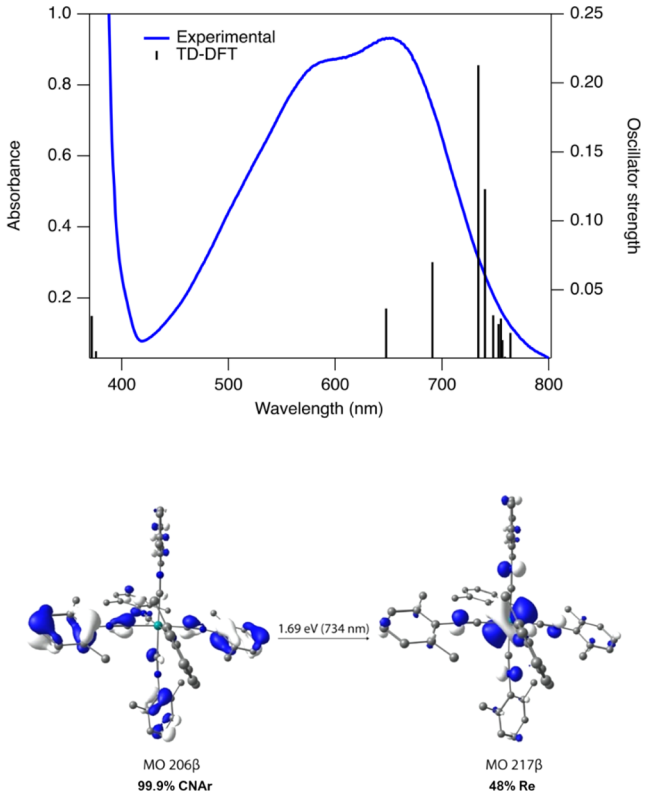

Figure 7. (Top) UV/vis absorbance spectra of 0.87 mM $[Re(CNAr)_6](PF_6)_2$ (blue) in CH_3CN (λ_{max} = 650 nm, ε = 1286 M^{-1} cm^{-1}), overlaid with computed vertical transitions in CH_3CN using PCM solvation (black). The vertical lines represent the vertical transitions predicted via TD-DFT. (Bottom) The donor (MO 206β) and acceptor (MO 217β) orbitals participating in the dominant LMCT, and transition with highest oscillator strength, at 734 nm (oscillator strength = 0.2127).

the electronic absorption spectrum of $[Re(CNAr)_6]^{2+}$, which was predicted implicitly in CH_3CN using the polarizable continuum model (PCM). The LMCT transition with the highest oscillator strength (734 nm) corresponds to a doublet−doublet transition from a ligand-based (CNAr) molecular orbital (HOMO − 10; MO 206β) to a Re-based orbital (β LUMO; MO 217β) (Figure 7). The TD-DFT predicted spectra agrees with the broad absorption observed experimentally for Re(II), but is red-shifted compared to experimental spectra (0.20 eV). Based on visual inspection (Figure 7) and population analysis,[33,34] the LMCT transition with the highest oscillator strength (f = 0.2127) which occurs at 734 nm, involves transfer of electron density from the CNAr π-orbitals (three CNAr ligands with 99% CNAr character) to the Re d-orbital (t_{2g}) with 48% Re character [π(CNAr) → dπ(M)]. Of the 99% character of the aryl isocyanide donor ligand, a significant contribution comes from the π-orbitals of the aryl ring—85% aryl ring versus 14% CN (see Table S5, Supporting Information). These data show that the lowest energy transition is not pure LMCT character but a mixture of LMCT and IL character similar to mixed MLCT/IL character observed for the Re(I) complex. The charge transfer reversal from MLCT to LMCT in Re(I) and Re(II) can be further rationalized with the orbital pictures of the respective charge transfers and the MO energy diagram (see Figures S13, S16, and S17). In Re(I), the charge transfer involves contributions from the HOMO and HOMO − 2 as donor orbitals (mixed ligand and d-orbital character) with the LUMO as the acceptor orbital (ligand-based). However, upon oxidation to form the d^5 Re(II) species, the half-filled d-orbital (β-LUMO) acts as the acceptor orbital which is then populated upon excitation from the low-lying ligand-based orbital.

The solid-state FTIR spectrum of the isolated $[Re(CNAr)_6](PF_6)_2$ has two ν(C≡N) stretches. A broad feature overlaps with the ν(C≡N) stretch observed for the Re(I) species at 2065 cm^{-1} and a new, slightly sharper feature is observed at 2121 cm^{-1} (Figure 8). Concerned that the feature at 2121 cm^{-1} indicated the presence of free ligand, formed through decomposition upon oxidation, rather than being representative of the Re(II) species, we sought additional support for assignment of the FTIR features of $[Re(CNAr)_6]^{2+}$. We employed IR spectroelectrochemistry to quantitatively monitor both the changes of ν(C≡N) bands and the stability of the complex through multiple cycle of

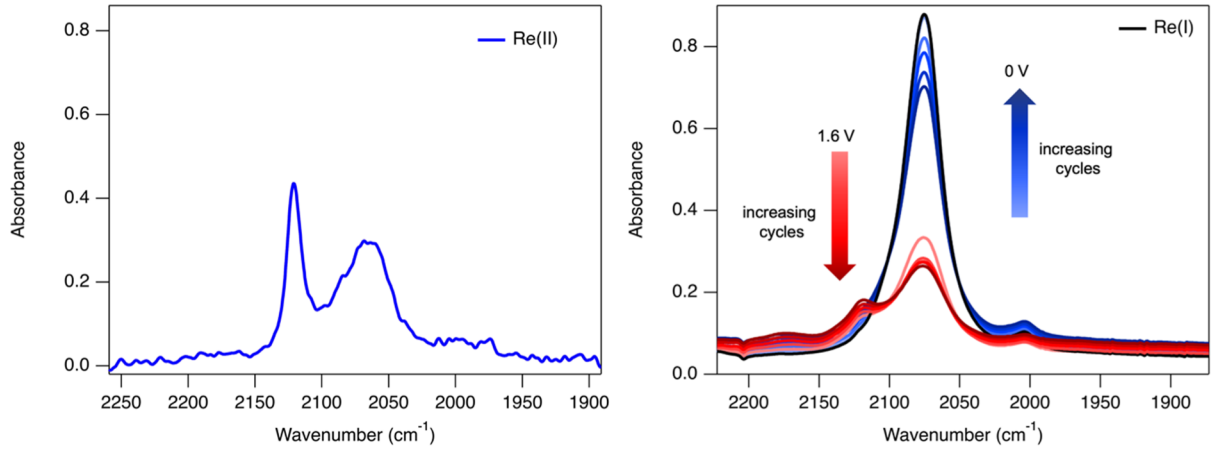

Figure 8. (Left) C≡N stretching region of the solid-state IR spectrum of $[Re(CNAr)_6](PF_6)_2$. Two IR stretches are observed, a higher energy stretch at 2121 cm^{-1} and a broad feature at 2065 cm^{-1} overlapping with the Re(I) C≡N stretching frequency. (Right) IR spectroelectrochemistry cycling experiments of $[Re(CNAr)_6]^+$ in CH_3CN. The cycles were performed by sequentially applying a potential capable of oxidizing Re(I) to Re(II) (1.6 V vs $Ag^{+/0}$, red traces) and a potential at which Re(II) would be reduced back to Re(I) (0 V vs $Ag^{+/0}$, blue traces). For each step, the potential was held for 60 s, and the absorbance spectra were recorded at the 8 s mark. The black trace is the Re(I) complex before the start of the experiment.

https://doi.org/10.1021/acs.inorgchem.2c03193
Inorg. Chem. 2023, 62, 6576−6585

sequential oxidation and reduction. In this experiment, the potential was stepped to potential positive of the Re(II/I) couple, held for 60 s, then stepped back to potential negative of the Re(II/I) couple (1.6 and 0 V vs $Ag^{+/0}$; due to experimental limitations of the spectroelectrochemical cell, the potential used was referenced vs the $Ag^{+/0}$ pseudo-reference electrode only; see the Experimental Section details above). The cycle was repeated five times, and an infrared absorbance spectrum was recorded at the 8 s point of each potential step. Upon stepping to a potential positive of the Re(II/I) couple, the growth of the feature ν(C≡N) at 2121 cm^{-1} is observed coupled to the partial bleach of the ν(C≡N) stretch at 2065 cm^{-1} (Figure 8). The subsequent step to potential negative of the Re(II/I) couple leads to the bleach of the 2121 cm^{-1} band and recovery of the 2065 cm^{-1} band. The bleach of the 2121 cm^{-1} band upon reduction indicates that this feature (as well as the lower intensity 2065 cm^{-1} band) can be attributed to the Re(II) species, not free ligand generated through the decomposition process, as the free ligand generated in decomposition would not bleach. However, although each subsequent cycle generates the same qualitative spectral changes, the absorbance of both spectral features slowly decreases with each cycle. We interpret these changes as decomposition of the Re(II) during the 60 s intervals, consistent with the stability of Re(II) described above. This observation of Re(II) decomposition helps explain the differences in intensity ratios of the 2121 and 2065 cm^{-1} bands in the steady-state and spectroelectrochemistry experiments; the steady-state sample may be contaminated by a decomposition product. Lastly, this spectroelectrochemical experiment indicates that the intensities of Re(II) IR absorbances are weaker than those of Re(I).

The reduction in symmetry observed crystallographically upon oxidation of $[Re(CNAr)_6]^+$ to $[Re(CNAr)_6]^{2+}$ was hypothesized to give rise to the split of the broad, intense 2065 cm^{-1} absorbance feature into two, low intensity infrared bands (see above). To interrogate this further, we employed DFT to compute the vibrational spectra of the $[Re(CNAr)_6]^{2+}$ complex, as described above for $[Re(CNAr)_6]^+$. This analysis indicates four IR-active C≡N stretching modes between 2165 and 2188 cm^{-1} with absorptivity between 713 and 1580 M^{-1} cm^{-1} (Figure S19). The shift in ν(C≡N) toward a higher frequency compared to the Re(I) calculations suggests a stronger C≡N bond consistent with weaker back-bonding between the Re t_{2g} and π^* orbitals of CNAr. An envelope was constructed by convoluting Gaussian functions centered over the stick spectra with a half-width at half-maximum of 7 cm^{-1}, qualitatively reproducing the experimental observation of two broad absorbance features. Furthermore, these calculations predict the experimentally observed weaker intensities of the ν(C≡N) bands for Re(II) as compared to Re(I). Collectively, both experimental and computational evidences point to the decrease in the IR intensity of the C≡N stretching modes due to subtle changes in the structure and reduction in symmetry going from Re(I) to Re(II).

CONCLUSIONS

The majority of transition-metal complexes supported by isocyanide ligands promote MLCT transitions with mixed ligand-centered character. Fewer examples reveal the role of isocyanide ligands as donors that engage in LMCT transitions.[8,19] In this work, spectroscopy and computational methods allow us to compare the electronic structures of $[Re(CNAr)_6]^+$ and $[Re(CNAr)_6]^{2+}$. Although the UV−vis absorbance spectrum of $[Re(CNAr)_6]^+$ is dominated by an MLCT transition mixed with IL character (λ_{max} = 300 nm) involving the π^* orbitals of the CNAr ligands, a broad absorbance in the visible region is observed for $[Re(CNAr)_6]^{2+}$ (λ_{max} = 650 nm), assigned to an LMCT transition with mixed IL character. The lowest energy LMCT vertical transition involves transition from an orbital with 99% ligand character (CNAr) to a metal d-orbital of 48% Re character. Importantly, the donor orbitals of the aryl isocyanide ligand engaging in this LMCT transition are identified for the first time, showing that a significant portion of the donor orbital is based on the aryl ring (85%) as opposed to the CN bond (14%). In the FTIR spectra of $[Re(CNAr)_6]^+$ and $[Re(CNAr)_6]^{2+}$, oxidation leads to a blue shift, splitting, and decrease in intensity of the ν(C≡N) stretch. X-ray crystallography and DFT calculations indicate that a reduction in symmetry at the metal center manifests in the decrease in intensity and split of the ν(C≡N) band. The blue shift in ν(C≡N) indicates less π-back-bonding from the higher Re(II) oxidation state. Collectively, these findings show that isocyanides can engage in LMCT transitions when coordinated to d^5 metal centers, while simultaneously serving as a reporter for the electron density at the metal center. The enhanced understanding of the orbital structure of aryl isocyanide ligands should increase opportunities to develop new photoactive complexes with LMCT excited states.

ASSOCIATED CONTENT

Supporting Information

The Supporting Information is available free of charge at https://pubs.acs.org/doi/10.1021/acs.inorgchem.2c03193.

^{1}H NMR, additional electrochemical data, high-resolution mass spectrometry, crystallographic data and details, additional IR spectra, UV−vis photostability measurements, and computational details (PDF)

Accession Codes

CCDC 2191910−2191911 contain the supplementary crystallographic data for this paper. These data can be obtained free of charge via www.ccdc.cam.ac.uk/data_request/cif, or by emailing data_request@ccdc.cam.ac.uk, or by contacting The Cambridge Crystallographic Data Centre, 12 Union Road, Cambridge CB2 1EZ, UK; fax: +44 1223 336033.

AUTHOR INFORMATION

Corresponding Authors

Elena Jakubikova − *Department of Chemistry, North Carolina State University, Raleigh, North Carolina 27695, United States;* orcid.org/0000-0001-7124-8300; Email: ejakubi@ncsu.edu

Jillian L. Dempsey − *Department of Chemistry, University of North Carolina at Chapel Hill, Chapel Hill, North Carolina 27599-3290, United States;* orcid.org/0000-0002-9459-4166; Email: dempseyj@email.unc.edu

Authors

Tayliz M. Rodriguez − *Department of Chemistry, University of North Carolina at Chapel Hill, Chapel Hill, North Carolina 27599-3290, United States*

Mawuli Deegbey − *Department of Chemistry, North Carolina State University, Raleigh, North Carolina 27695, United States;* orcid.org/0000-0003-4478-3353

https://doi.org/10.1021/acs.inorgchem.2c03193
Inorg. Chem. 2023, 62, 6576−6585

Chun-Hsing Chen − *Department of Chemistry, University of North Carolina at Chapel Hill, Chapel Hill, North Carolina 27599-3290, United States;* orcid.org/0000-0003-0150-9557

Complete contact information is available at: https://pubs.acs.org/10.1021/acs.inorgchem.2c03193

Author Contributions

The manuscript was written through contributions of all authors.

Notes

The authors declare no competing financial interest.

■ ACKNOWLEDGMENTS

This work was supported by the National Science Foundation for both experimental (CHE-1954868) and theoretical (CHE-1554855) aspects of this project. T.M.R. acknowledges support from the National Science Foundation Graduate Research Fellowship (DGE-1650116). J.L.D. acknowledges support from a Packard Fellowship for Science and Engineering. We acknowledge use of the X-ray diffractometer at the Molecular Education, Technology and Research Innovation Center (METRIC) at NC State University, instrumentation in the Mass Spectrometry Core Laboratory supported by the National Science Foundation (CHE-1726291), and the NMR Core Facility. We also gratefully acknowledge the computing resources provided by North Carolina State University High Performance Computing Services Core Facility (RRID:SCR_022168). We thank Eric Assaf, Sara Gebre, Jennica Kelm, Tianquan Lian, Andrew Moran, Mac McNamee, and Renato Sampaio for insightful discussion and experimental assistance. Finally, we also acknowledge Matthew Verber and Regent Joubert from the UNC Chemistry Electronics Shop for assisting in troubleshooting and repairing the IR spectroelectrochemistry cell.

■ REFERENCES

(1) Cotton, A.; Zingales, F. The Donor-Acceptor Properties of Isonitriles as Estimated by Infrared Study. *J. Am. Chem. Soc.* **1961**, *83*, 351−355.

(2) Carpenter, A. E.; Mokhtarzadeh, C. C.; Ripatti, D. S.; Havrylyuk, I.; Kamezawa, R.; Moore, C. E.; Rheingold, A. L.; Figueroa, J. S. Comparative Measure of the Electronic Influence of Highly Substituted Aryl Isocyanides. *Inorg. Chem.* **2015**, *54*, 2936−2944.

(3) Drance, M. J.; Figueroa, J. S. Low-Coordinate Manganese Complexes Perform Unusual Bond-Formation Reactions. *Chem* **2018**, *4*, 2734−2736.

(4) Claude, G.; Salsi, F.; Hagenbach, A.; Gembicky, M.; Neville, M.; Chan, C.; Figueroa, J. S.; Abram, U. Structural and Redox Variations in Technetium Complexes Supported by M-Terphenyl Isocyanides. *Organometallics* **2020**, *39*, 2287−2294.

(5) Salsi, F.; Neville, M.; Drance, M.; Hagenbach, A.; Chan, C.; Figueroa, J. S.; Abram, U. A Closed-Shell Monomeric Rhenium(1-) Anion Provided by: M-Terphenyl Isocyanide Ligation. *Chem. Commun.* **2020**, *56*, 7009−7012.

(6) Margulieux, G. W.; Weidemann, N.; Lacy, D. C.; Moore, C. E.; Rheingold, A. L.; Figueroa, J. S. Isocyano Analogues of $[Co(CO)_4]^n$: A Tetraisocyanide of Cobalt Isolated in Three States of Charge. *J. Am. Chem. Soc.* **2010**, *132*, 5033−5035.

(7) Emerich, B. M.; Moore, C. E.; Fox, B. J.; Rheingold, A. L.; Figueroa, J. S. Protecting-Group-Free Access to a Three-Coordinate Nickel(0) Tris-Isocyanide. *Organometallics* **2011**, *30*, 2598−2608.

(8) Mann, K. R.; Cimolino, M.; Geoffroy, G. L.; Hammond, G. S.; Orio, A. A.; Albertin, G.; Gray, H. B. Electronic Structures and Spectra of Hexakisphenylisocyanide Complexes of Cr(0), Mo(0), W(0), Mn(I), and Mn(II). *Inorg. Chim. Acta* **1976**, *16*, 97−101.

(9) Arias-Rotondo, D. M.; McCusker, J. K. The Photophysics of Photoredox Catalysis: A Roadmap for Catalyst Design. *Chem. Soc. Rev.* **2016**, *45*, 5803−5820.

(10) Thompson, D. W.; Ito, A.; Meyer, T. J. $[Ru(bpy)_3]^{2+*}$ and Other Remarkable Metal-to-Ligand Charge Transfer (MLCT) Excited States. *Pure Appl. Chem.* **2013**, *85*, 1257−1305.

(11) Harris, J. P.; Reber, C.; Colmer, H. E.; Jackson, T. A.; Forshaw, A. P.; Smith, J. M.; Kinney, R. A.; Telser, J. Near-Infrared $^2E_g \rightarrow {}^4A_{2g}$ and Visible LMCT Luminescence from a Molecular Bis-(Tris-(Carbene)Borate) Manganese(IV) Complex. *Can. J. Chem.* **2017**, *95*, 547−552.

(12) Dorn, M.; Kalmbach, J.; Boden, P.; Päpcke, A.; Gómez, S.; Förster, C.; Kuczelinis, F.; Carrella, L. M.; Büldt, L. A.; Bings, N. H.; Rentschler, E.; Lochbrunner, S.; González, L.; Gerhards, M.; Seitz, M.; Heinze, K. A Vanadium(III) Complex with Blue and NIR-II Spin-Flip Luminescence in Solution. *J. Am. Chem. Soc.* **2020**, *142*, 7947−7955.

(13) Zhang, Y.; Lee, T. S.; Favale, J. M.; Leary, D. C.; Petersen, J. L.; Scholes, G. D.; Castellano, F. N.; Milsmann, C. Delayed Fluorescence from a Zirconium(IV) Photosensitizer with Ligand-to-Metal Charge-Transfer Excited States. *Nat. Chem.* **2020**, *12*, 345−352.

(14) Chábera, P.; Liu, Y.; Prakash, O.; Thyrhaug, E.; Nahhas, A. E.; Honarfar, A.; Essén, S.; Fredin, L. A.; Harlang, T. C. B.; Kjær, K. S.; Handrup, K.; Ericson, F.; Tatsuno, H.; Morgan, K.; Schnadt, J.; Häggström, L.; Ericsson, T.; Sobkowiak, A.; Lidin, S.; Huang, P.; Styring, S.; Uhlig, J.; Bendix, J.; Lomoth, R.; Sundström, V.; Persson, P.; Wärnmark, K. A Low-Spin Fe(III) Complex with 100-ps Ligand-to-Metal Charge Transfer Photoluminescence. *Nature* **2017**, *543*, 695−699.

(15) Adams, J. J.; Arulsamy, N.; Sullivan, B. P.; Roddick, D. M.; Neuberger, A.; Schmehl, R. H. Homoleptic Tris-Diphosphine Re(I) and Re(II) Complexes and Re(II) Photophysics and Photochemistry. *Inorg. Chem.* **2015**, *54*, 11136−11149.

(16) Zhang, Y.; Akhmedov, N. G.; Petersen, J. L.; Milsmann, C. Photoluminescence of Seven-Coordinate Zirconium and Hafnium Complexes with 2,2′-Pyridylpyrrolide Ligands. *Chem.—Eur. J.* **2019**, *25*, 3042−3052.

(17) Li, C.; Kong, X. Y.; Tan, Z. H.; Yang, C. T.; Soo, H. Emergence of Ligand-to-Metal Charge Transfer in Homogeneous Photocatalysis and Photosensitization. *Chem. Phys. Rev.* **2022**, *3*, 021303.

(18) Chábera, P.; Lindh, L.; Rosemann, N. W.; Prakash, O.; Uhlig, J.; Yartsev, A.; Wärnmark, K.; Sundström, V.; Persson, P. Photofunctionality of Iron(III) N-Heterocyclic Carbenes and Related d^5 Transition Metal Complexes. *Coord. Chem. Rev.* **2021**, *426*, 213517.

(19) Alexander, J. J.; Gray, H. B. Electronic Structures of Hexacyanometalate Complexes. *J. Am. Chem. Soc.* **1968**, *90*, 4260−4271.

(20) Chábera, P.; Kjaer, K. S.; Prakash, O.; Honarfar, A.; Liu, Y.; Fredin, L. A.; Harlang, T. C. B.; Lidin, S.; Uhlig, J.; Sundström, V.; Lomoth, R.; Persson, P.; Wärnmark, K. Fe(II) Hexa N-Heterocyclic Carbene Complex with a 528 ps Metal-To-Ligand Charge-Transfer Excited-State Lifetime. *J. Phys. Chem. Lett.* **2018**, *9*, 459−463.

(21) Cadranel, A.; Gravogl, L.; Munz, D.; Meyer, K. Intense Photoinduced Intervalence Charge Transfer in High-Valent Iron Mixed Phenolate/Carbene Complexes. *Chem.—Eur. J.* **2022**, *28*, No. e202200269.

(22) Villegas, J. M.; Stoyanov, S. R.; Reibenspies, J. H.; Rillema, D. P. Spectroscopic and Computational Investigations of the Temperature-Dependent Emission Behavior of $[Re(CNx)_5Cl]$ and $[Re(CNx)_6]^+$ Complexes. *Organometallics* **2005**, *24*, 395−404.

(23) Boduszek, B.; Shine, H. J. Preparation of Solid Thianthrene Cation Radical Tetrafluoroborate. *J. Org. Chem.* **1988**, *53*, 5142−5143.

(24) Krejčik, M.; Daněk, M.; Hartl, F. Simple Construction of an Infrared Optically Transparent Thin-Layer Electrochemical Cell. *J. Electroanal. Chem. Interfacial Electrochem.* **1991**, *317*, 179−187.

(25) Blessing, R. H. An Empirical Correction for Absorption Anisotropy. *Acta Crystallogr., Sect. A: Found. Crystallogr.* **1995**, *51*, 33−38.
(26) Sheldrick, G. M. SHELXT - Integrated Space-Group and Crystal-Structure Determination. *Acta Crystallogr., Sect. A: Found. Crystallogr.* **2015**, *71*, 3−8.
(27) Betteridge, P. W.; Carruthers, J. R.; Cooper, R. I.; Prout, K.; Watkin, D. J. CRYSTALS Version 12: Software for Guided Crystal Structure Analysis. *J. Appl. Crystallogr.* **2003**, *36*, 1487.
(28) Ossinger, S.; Prescimone, A.; Häussinger, D.; Wenger, O. S. Manganese(I) Complex with Monodentate Arylisocyanide Ligands Shows Photodissociation Instead of Luminescence. *Inorg. Chem.* **2022**, *61*, 10533−10547.
(29) Verdonck, L.; Tulun, T.; van der Kelen, G. P. Far IR and Raman Spectra of $(RNC)_6Mn^+$ Compounds (R = CH_3, C_6H_5, 4-Cl—C_6H_4). *Spectrochim. Acta, Part A* **1979**, *35*, 867−870.
(30) Alecu, I. M.; Zheng, J.; Zhao, Y.; Truhlar, D. G. Computational Thermochemistry: Scale Factor Databases and Scale Factors for Vibrational Frequencies Obtained from Electronic Model Chemistries. *J. Chem. Theory Comput.* **2010**, *6*, 2872−2887.
(31) Herr, P.; Kerzig, C.; Larsen, C. B.; Häussinger, D.; Wenger, O. S. Manganese(I) Complexes with Metal-to-Ligand Charge Transfer Luminescence and Photoreactivity. *Nat. Chem.* **2021**, *13*, 956−962.
(32) Connelly, N. G.; Geiger, W. E. Chemical Redox Agents for Organometallic Chemistry. *Chem. Rev.* **1996**, *96*, 877−910.
(33) Gorelsky, S. I.; Lever, A. B. P. Electronic Structure and Spectra of Ruthenium Diimine Complexes by Density Functional Theory and INDO/S. Comparison of the Two Methods. *J. Organomet. Chem.* **2001**, *635*, 187−196.
(34) Gorelsky, S. I. *AOMix.pdf*.

https://doi.org/10.1021/acs.inorgchem.2c03193
Inorg. Chem. 2023, 62, 6576−6585